encit 2020

ABCM
Associação Brasileira de Engenharia e Ciências Mecânicas

18th Brazilian Congress of Thermal Sciences and Engineering
November 16–20, 2020 (Online)

ENC-2020-0057
NUMERICAL INVESTIGATION OF THE EFFECTS OF DIFFERENT CONSTITUTIVE RHEOLOGY MODELS ON BLOOD FLOW TOPOLOGY

Gustavo P. V. Almeida
Instituto Tecnológico de Aeronáutica - ITA
gupalmeida@gmail.com

João Luiz F. Azevedo
Instituto de Aeronáutica e Espaço - IAE
joaoluiz.azevedo@gmail.com

Abstract. *The application of CFD to understand mechanical flow properties in complex flows plays a vital role in hemodynamics. The viscosity of the blood is mainly dependent of the volume fraction of red blood cells and plasma in its composition, and how much these blood cells are deformed as a function of the flow field. Hence, blood structure may lead to a non-Newtonian behavior under certain flow conditions. The present work evaluate the effects of Generalized Newtonian Fluid (GNF) constitutive rheology models on the flow field for blood flowing through a constricted channel using OpenFOAM libraries. Results have proven the sensitivity of flow field to the yield stress with variations in velocity magnitudes up to 6.3% and in Wall Shear Stress (WSS) up to 16.17%.*

Keywords: *Rheology, Blood viscosity, CFD, Non-Newtonian Fluid, OpenFOAM*

1. INTRODUCTION

Computational Fluid Dynamics (CFD) techniques are evolving and their application are spreading for many different fields of science (Hirsch, 1990; Moukalled *et al.*, 2016). The CFD techniques consist fundamentally of applying numerical algorithms to solve equations of fluid motion, allowing to evaluate complex fluid flow phenomena. Complexities observed in fluid dynamics problems such as turbulence, non-linearity in fluid viscosity (rheology model), transient and non-stationary effects motivate the application of CFD in fields such as in hemodynamics, oil and gas, aerodynamics, etc (Wilcox, 2006; Rosenfeld, 1993; Paul and Molla, 2012). The main idea behind numerical simulations is to quantify flow properties such as velocity and pressure fields, shear stresses and temperature distributions, as well as to obtain flow visualization where the application of analytical or experimental procedures are either not possible or prohibitively expensive.

The application of numerical methods for simulating the blood flow in human body is commonly known as Computational Hemodynamics (CHD) (Tu *et al.*, 2015). These techniques have been applied in the last decades in order to provide a better understanding of the blood flow properties and topology. Moreover, the increasing interest in applying numerical techniques for quantitative medical diagnostics in order to predict possible cardiovascular diseases have been leading the scientific community to deeply study the subject (Mittal *et al.*, 2016). Therefore, high-fidelity models in many different spatial and temporal scales, as well as precise rheology models for modeling blood flow are some of the current challenges to be explored by researchers (Cebral *et al.*, 2007; Farina *et al.*, 2018).

The studies on the influence of rheology models and time-dependent boundary conditions over blood flow properties such as Wall Shear Stresses (WSS), velocity field and pressure gradients play an important role in hemodynamics. The main idea relies on using CFD results as means of non-invasive medical imaging technique combined with the current available qualitative state-of-the-art medical features in the process of diagnosing cardiovascular pathologies (Wong and Poon, 2011; Mittal *et al.*, 2016). Many studies have been performed in an attempt of establishing a correlation between the blood flow properties and the development of the most critical cardiovascular diseases such as stenosis and aneurysms (Paul and Molla, 2012; Piskin and Celebi, 2013; Pinto *et al.*, 2013; Mamun *et al.*, 2015). Some researches reveal these cardiovascular diseases may be evaluated through the use of CFD prior to any surgical intervention.

The hypothesis of assuming the blood as a Newtonian fluid in hemodynamics simulations is sometimes made in order to simplify the models. Such an assumption is supported by the observations of only small variations on the blood flow field under certain flow conditions, as stated by Tu *et al.* (2015); Farina *et al.* (2018); Mittal *et al.* (2016). However, the blood is fundamentally a suspension of red blood cells in plasma, whose viscosity is mainly dependent of their volume fraction and how much these blood cells are deformed in function of the flow field. In other words, the viscosity of the

blood may change depending on whether the flow experiences large variations in pressure gradients, velocity fields and WSS. Therefore, neglecting these effects may jeopardize the analysis. Hence, the choice of the constitutive rheology model may, in fact, impact the final results in hemodynamic simulations and the non-Newtonian assumption should be made in order to obtain accurate high-fidelity results (Farina *et al.*, 2018; Almeida and Azevedo, 2017, 2018).

The constricted channel is chosen for the present study given its suitability for validation in many applications. The jet-like flow characteristics downstream of the constriction is of wide use for studies related to flow detachment-reattachment, moving vortices and pressure drop analyses. For instance, in hemodynamics the constricted channel represents an ill blood vessel with a narrowed flow area due to the accumulation of plaque. The main goal of this work is to present a study on the effects of different constitutive rheology models for blood flowing in a constricted channel using OpenFOAM libraries. The results for two Generalized Newtonian Fluid (GNF) viscosity models are compared, namely the power-law and the Herschel-Bulkley. The effects of shear thinning effects on blood flow quantities are discussed hereafter.

2. THEORETICAL AND NUMERICAL FORMULATIONS

The authors have chosen to use the OpenFOAM (Weller *et al.*, 1998; OpenCFD, 2016) open source libraries for the numerical simulations of the flows of interest due to their readiness and customizability, as well as their wide applicability for numerous models of fluid flows. The geometry is constructed using a simple idealized constricted channel shape mainly because of its highly applicability in hemodynamic studies for modeling deformed blood vessels. The authors describe here the theoretical and numerical formulations which are embedded in the tool used, with emphasis on the issues associated to the rheology constitutive models.

2.1 Theoretical Model

The governing equations of motion for incompressible fluids are given by the Navier-Stokes equations. These equations can be written as

$$\frac{\partial u_j}{\partial x_j} = 0 \tag{1}$$

and

$$\frac{\partial(\rho u_i)}{\partial t} + \frac{\partial(\rho u_i u_j)}{\partial x_j} = -\frac{\partial p}{\partial x_i} + \frac{\partial \tau_{ij}}{\partial x_j}\,, \tag{2}$$

where u_j and u_i are the $j-th$ and $i-th$ components of the velocity vector, respectively; ρ is the fluid density and τ_{ij} is the $ij-th$ component of the viscous stress tensor. The linear relation between shear stresses and shear strain rate for an incompressible Newtonian fluid is given by

$$\tau_{ij} = 2\mu_{eff} s_{ij}\,, \tag{3}$$

where s_{ij} is the $ij-th$ component of the strain tensor and μ_{eff} is the effective fluid viscosity coefficient, which turns out to be a constant, $\mu_{Newtonian}$, for the Newtonian fluid viscosity model. The strain tensor, described in Eq. (3), may be written as a function of the velocity field as

$$s_{ij} = \frac{1}{2}\left(\frac{\partial u_i}{\partial x_j} + \frac{\partial u_j}{\partial x_i}\right)\,. \tag{4}$$

The non-Newtonian viscosity models, in the other hand, present a non-linear relation between shear stresses and the strain rate. There are many models available in the literature. The authors, however, choose to adopt two most commonly used for modeling blood and blood-like fluid viscosity in the present studies. These two models are referred to in the literature as GNF models. The first one, namely the Herschel-Bulkley model, belongs to a group of models the authors refer to here as the yield stress models (Valencia *et al.*, 2007; Kim, 2002; Farina *et al.*, 2018). The second group is a derivation of the yield stress model, in the sense they do not present an yield stress and, therefore, are known simply as general power-law fluids. The fluid behavior for each of these models is illustrated in Fig. (1). The authors encourage the readers to look at studies which present results for rheology models differing from those used here, including the rationales for the choice of each model (Calafati, 2010; Brambatti, 2010).

The magnitude of the strain rate, $\dot{\gamma}$, is given by definition as a function of the velocity field for the non-linear models. The relation between the magnitude of the strain rate and the flow velocity field is written as

$$\dot{\gamma} = \sqrt{2 s_{ij} s_{ij}}\,. \tag{5}$$

The general equation for the Herschel-Bulkley fluid viscosity model is given by

$$\mu_{eff} = k\dot{\gamma}^{n-1} + \frac{\tau_0}{\dot{\gamma}}, \tag{6}$$

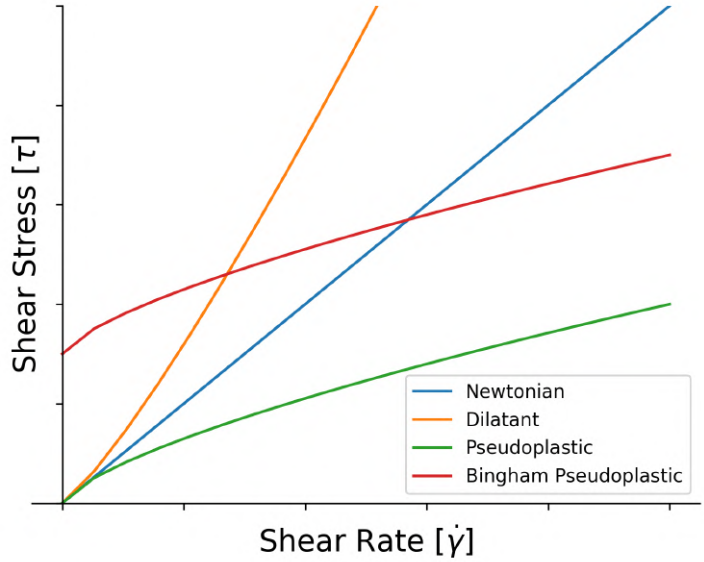

Figure 1. Shear stress, τ, as a function of strain rate, $\dot{\gamma}$

where k is a constant of proportionality also known as fluid consistency index, n is the dimensionless flow index, and τ_0 is the yield stress. The flow index indicates whether the fluid behaves like a shear-thinning (pseudo-plastic) or shear-thickening (dilatant) fluid. In scenarios where the non-Newtonian effects are observed, the blood presents a shear-thinning behavior, with $n < 1$. This means that the fluid viscosity decreases as the shear strain rate increases. Values of k and n for modeling blood viscosity are easily found in the literature (Tu *et al.*, 2015; Farina *et al.*, 2018).

The power-law fluid model, as previously mentioned, presents no yield stress and, therefore, Eq. (6) is simply reduced to

$$\mu_{eff} = k\dot{\gamma}^{n-1} \, . \tag{7}$$

Equations (6) and (7) clearly show that for $n = 1$ and $\tau_0 = 0$ the model reconstitutes the original Newtonian formulation, with $k = \mu_{Newtonian}$. In order to keep consistency in the nomenclature, the case in which the Herschel-Bulkley fluid model assumes the aforementioned values of yield stress and fluid index will be referred to simply as GNF model in the remaining of the text.

The general form for the Reynolds number and the fully developed velocity profile in the channel are represented, respectively, by

$$Re = \frac{\rho U^{2n} L^n}{\left[\frac{8^{n-1}k(3n+1)}{4n}\right]^n} \, , \tag{8}$$

and

$$U(r) = U_{avg}\left(\frac{3n+1}{n+1}\right)\left[1 - \left(\frac{r}{R}\right)^{\frac{n+1}{n}}\right] \, . \tag{9}$$

In Eq. (8) ρ is the fluid density, U is a characteristic velocity and L is a characteristic length, whereas in Eq. (9) U_{avg} is the average flow velocity, r is an arbitrary position in radial direction and R is the channel radius. Intuitively, Eq. (8) and Eq. (9) reconstitute the well known form of these equations when $n = 1$ and $k = \mu_{Newtonian}$, where $\mu_{Newtonian}$ is the Newtonian fluid viscosity coefficient (Galdi *et al.*, 2008).

In contrast with the Reynolds number, Re, which establishes a relation between inertial and viscous forces, the Bingham number, Bn, defines a relation between the yield stress and viscous forces. The dimensionless Bingham number is defined as

$$Bn = \frac{\tau_0 L}{\mu_{eff} U} \, . \tag{10}$$

The Bingham number is commonly used when modeling fluid flows with the yield stress viscosity models.

As previously mentioned the red blood cells volume fraction may cause the blood to flow like a non-Newtonian fluid. Additionally, depending on the concentration of red blood cells in the plasma, the blood flow may, in fact, face an yield

stress and, consequently, behave like a solid for a given strain rate (Farina *et al.*, 2018). Hence, most of the times, the choice of an yield stress model is preferred between those available for the application of interest.

2.2 Numerical Formulation

The OpenFOAM is a set of numerical libraries written in C++ language which encapsulates, in its own namespace, ways of performing vectorial and tensorial calculus. The libraries used to solve problems of fluid dynamics make use of the Finite Volume Method (FVM) (Moukalled *et al.*, 2016) for discretization of the transport equations for the problem of interest. There are several solvers available in the OpenFOAM library. However, the authors have chosen the *pisoFoam* application (Almeida and Azevedo, 2017, 2018).

There are several numerical schemes available for each term of the governing equations for the problem of interest. The spatial terms of the equations are discretized and solved using a simple Gauss linear scheme. In other words, the integration of properties along the cell boundaries is made using the Gauss quadrature method with only one integration point, leading to a second order accuracy scheme for the spatial terms Moukalled *et al.* (2016). The numerical schemes available in the OpenFOAM libraries for temporal discretization are all implicit methods. The authors, however, have chosen to run a steady-state simulation. The PISO algorithm is used for solving the pressure-momentum coupling.

The implementation of the non-Newtonian viscosity models in OpenFOAM follows a simple approach. As described in OpenCFD (2016), the models basically computes the viscosity behavior as per Eqs. (6) and (7). Additionally, given pisoFoam is used for solving incompressible flow problems, the solver uses the kinematic viscosity, ν_{eff}, rather than the effective viscosity, mu_{eff}. The kinematic viscosity is obtained simply as a ratio between the effective dynamic viscosity and the fluid density, ρ.

To deal with problems of singularity in the viscosity models used, the OpenFOAM truncates the viscosity to minimum and a maximum values for when the strain rate reaches 0 and ∞, respectively. Hence, the power-law and the Herschel-Bulkley viscosity models limits implemented in OpenFOAM are given by

$$\nu_{min} \leq \nu_{eff} \leq \nu_{max} \text{ , and} \tag{11}$$

$$\nu_{eff} = min(\nu_0, k\dot{\gamma}^{n-1} + \frac{\tau_0}{\dot{\gamma}}) \, . \tag{12}$$

As stated above, the kinematic viscosity, ν_{eff}, is used by the incompressible flow solver pisoFoam. It is, therefore, worth mentioning that both the fluid consistency index, k, and the yield stress, τ_0 are also given as ratios by the fluid density, ρ.

2.3 Simulation Procedure

The simulations are divided in 6 different cases. The cases prepared for comparing the flow topology are given in Table 1. One single idealized constriction is adopted and the flow is assumed to be at a fixed Reynolds number, $Re = 100$, in all cases.

Table 1. Summary of cases setup

Case No.	Rheology Model	d/D	Bn	n	k $[m^2/s^{n-1}]$
1	GNF	0.7	0	1	2.86e-05
2	Power-Law	0.7	0	0.7755	0.1482
3	Herschel-Bulkley	0.7	0	0.7755	0.1482
4	Herschel-Bulkley	0.7	1	0.7755	0.1482
5	Herschel-Bulkley	0.7	10	0.7755	0.1482
6	Herschel-Bulkley	0.7	20	0.7755	0.1482

The geometry is exemplified in Figure 2. The relation between diameters used is such that the area of the small diameter halves the area of the pipe. Hence $d/D = 0.7$. The total length of the channel is 105 mm with the throat of the constriction located at half of the channel length. The blood density is assumed to be 1060 kg/m^3. Values of consistency index, k, and flow index, n, for blood are taken from literature (Walburn and Schneck, 1976; Kim *et al.*, 2000; Kim, 2002; Farina *et al.*, 2018). The value of the kinematic viscosity at zero strain rate, ν_0, is obtained by simply extrapolating the resulting curve using the values of k and n for the worst case, $Bn = 20$. The authors have chosen a single reference value for each of the mentioned parameters in order to provide insight of the model sensitivity regarding purely the yield stress over the flow topology (Farina *et al.*, 2018; Valencia *et al.*, 2006). Besides, a zero Bingham number case, $Bn = 0$, is run for the Herschel-Bulkley viscosity model in order to check for numerical effects due to a slight difference in the model limits implementation in the OpenFOAM source code with respect to the power-law model.

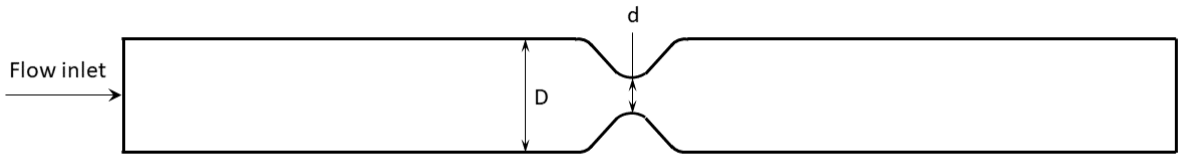

Figure 2. Constricted channel geometry

A fixed parabolic laminar velocity profile, with an average velocity of 49.06 cm/s, is imposed as boundary condition at the inlet with a zero velocity gradient imposed at the outlet for all the models. Even though the application of the same parabolic velocity profile at the inlet for the non-Newtonian models may not be ideal, that represents a reasonable starting point (Johnston *et al.*, 2004). A fixed reference gauge pressure is imposed at the outlet with an extrapolation of the pressure from the interior of the computational domain to the inlet boundary. Rigid walls are assumed with no slip boundary condition.

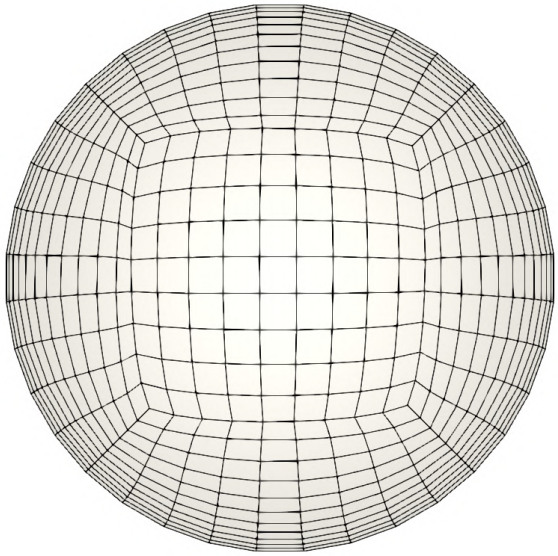

Figure 3. Inlet mesh topology of the constricted channel

The computational mesh is constructed using a multi-block strategy with hexahedral volumes and a final resolution of 121,635 cells for the entire domain. Figure 3 depicts a typical mesh topology for inlet of channel, presenting a total of 477 faces and 496 nodes. No symmetry plane is used to reduce computational effort given the total number of cells for the cases is relatively small.

3. RESULTS

The distribution of the velocity magnitudes in the radial direction as well as at the center line of the channel, shown respectively in Figs. 4 and 5, are normalized. The normalization of the velocity magnitudes takes into account the average velocity imposed as boundary condition. The computed velocity magnitudes have shown perfect match between the Newtonian and the GNF viscosity model along all the computational domain, when the former is given for fluid parameters $n = 1$ and $k = \mu_{Newtonian}$. Such result validates the hypothesis of reconstituting the Newtonian fluid viscosity by imposing the proper parameters to the GNF viscosity models. This behavior is observed both for the distribution of the velocity magnitudes in the radial direction taken upstream of the constriction, shown in Fig. 4, and along the center line of the channel, shown in Fig. 5. The distribution of the velocity magnitude for the GNF model, represented by the blue dashed lines, lies exactly over the curve plot for the Newtonian fluid model, represented by the black line.

As for any internal flow, the velocity magnitude reaches its maximum value at the center of the duct, given the development of the flow within the duct. Probing the velocity magnitudes along the center line of the channel, the non-Newtonian fluid models presented smaller values when compared to the Newtonian fluid, as expected. Despite the small difference in the source code implementation, Herschel-Bulkley and Power-law viscosity models are in agreement when

the first one is used adopting zero yield stress, $\tau_0 = 0$. As expected, the power-law fluid behavior is given as a sub-set of the Herschel-Bulkley fluid when the later is given for the same fluid index and consistency index at a zero yield stress condition.

The reduction in maximum velocity becomes more evident when the fluid flows under higher Bingham numbers for the Herschel-Bulkley fluid model. The velocity profiles in Fig. 4 show the flattened curves for the non-Newtonian fluids, as expected. As the boundary condition imposes a constant strain rate for a given fixed velocity profile at the inlet of the domain, the shear thinning behavior of the non-Newtonian fluid leads to a lower viscosity. As a consequence, the slope of the velocity profile is not as steep if compared to the Newtonian fluid and, therefore, the velocity profile becomes flattened. The observed behavior validates the hypotheses that for a given strain rate, $\dot{\gamma}$, the fluid will face a higher resistance to flow and, consequently, the maximum velocity magnitude at the centerline of the duct decreases along its whole length.

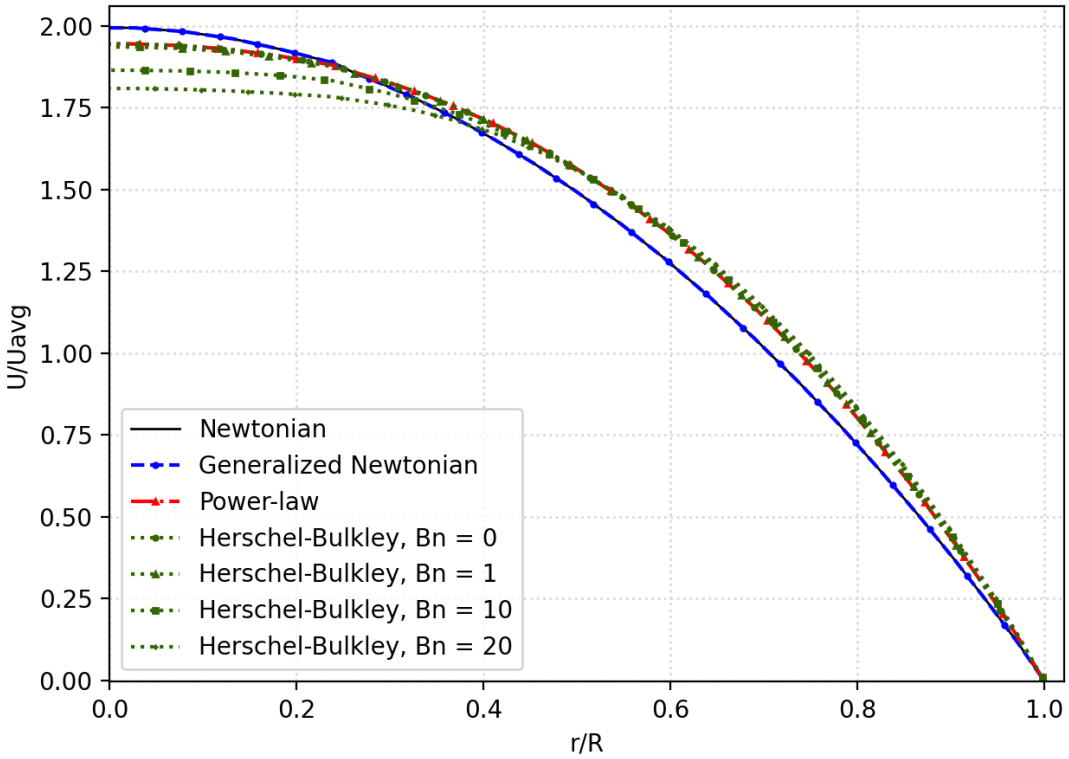

Figure 4. Distribution of velocity magnitude in the radial direction

The most significant differences occur when the flow regime is under higher Bingham numbers. Figure 6 reveals the trend of decreasing the flow velocity magnitude as the Bingham number increases. The maximum velocity magnitude for case 6 presents a reduction of approximately 6.3% compared to the unyielded flow in case 3 and 8.5% if compared to the Newtonian fluid. It is worth mentioning that these results are obtained for a flow at low Reynolds number, $Re = 100$, and such differences in the velocity magnitude between all fluid models may significantly vary with either higher values of Reynolds number or even for oscillating flow conditions.

The contour plots for velocity magnitude are depicted in Fig. 7. All velocity contour plots are given in the same normalized color scale to make visualization meaningful. The first plot at the top presents the results for the Newtonian case and it is used as baseline for setting the color scale. The subsequent six velocity contour plots illustrate the other simulated cases given in the same order as indicated in Tab. 1. The flow acceleration caused by the change in geometry creates a jet-like flow topology downstream of the constricted region with its maximum velocity reached at the throat of the constriction. As the results are obtained for a flow at a very low Reynolds number, *i.e.*, $Re = 100$, differences in the velocity contours for all the models are barely visible. Nonetheless, a smooth flow downstream of the constriction is consistently observed in all the cases and no recirculation occurs in the flow. Increasing local Reynolds number by either increasing the overall flow velocity or by making a more severe narrowing in the model geometry would induce flow recirculation zones downstream of the constriction as presented by Almeida and Azevedo (2018).

Table 2 shows the variation in the maximum Wall Shear Stress (WSS) for each simulated case in comparison to the Newtonian model. Again, the GNF case, *i.e.*, case 1, perfectly matches the results of the Newtonian fluid for which the viscosity is a constant coefficient with no variation in the computed WSS. The variations occur for the models in which the shear-thinning behavior is present. Differences in the WSS range from 13.26% to 16.17% in comparison with the

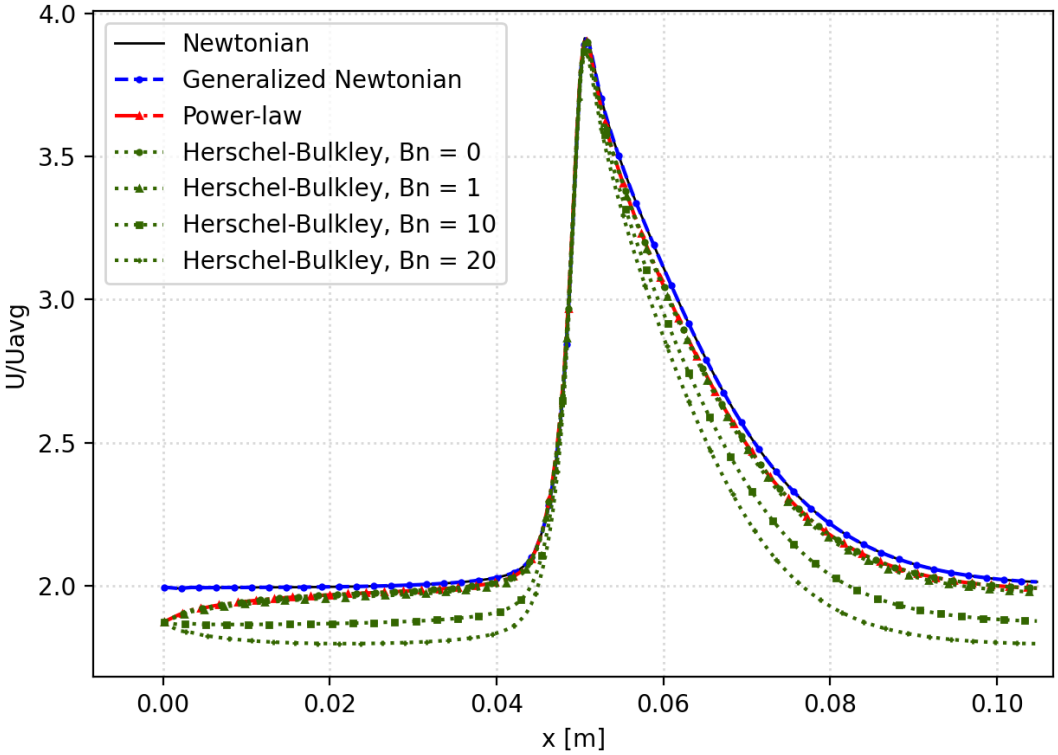

Figure 5. Velocity magnitudes at the centerline along the whole channel length

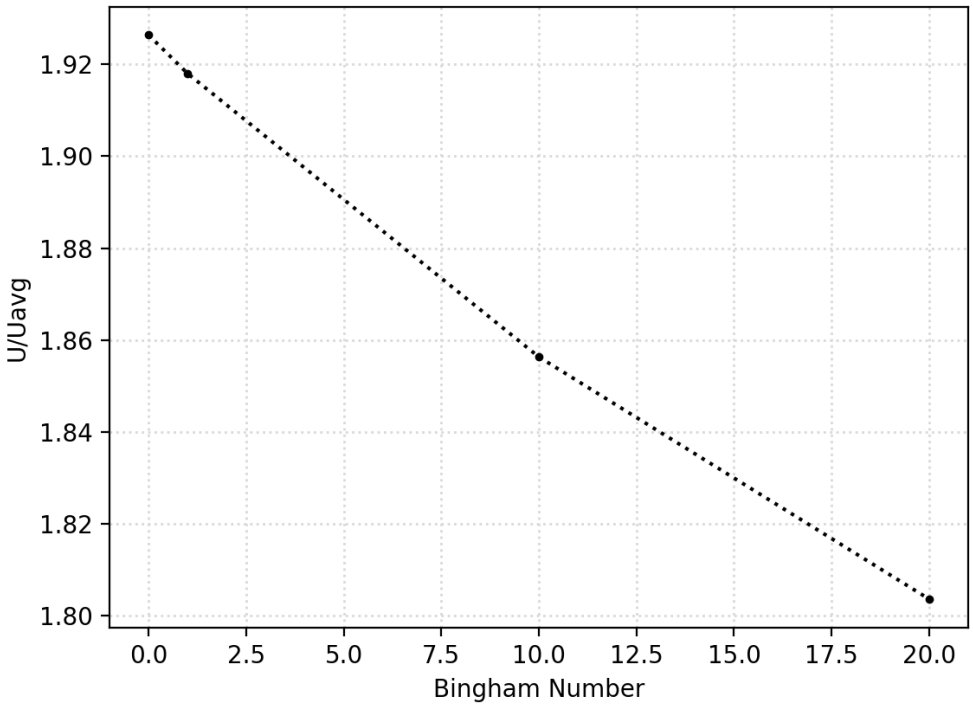

Figure 6. Maximum velocity magnitude at the centerline of the channel in the inlet plane as a function of Bingham number

Newtonian fluid model.

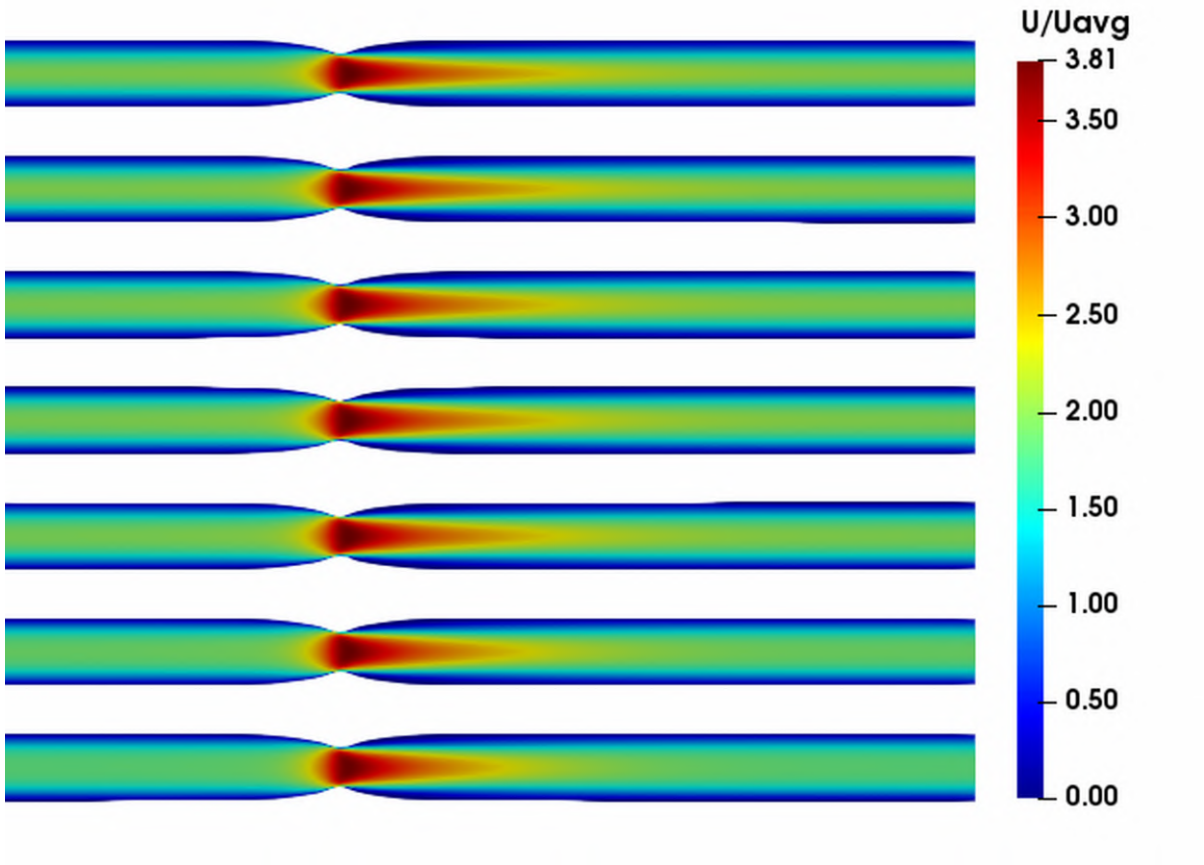

Figure 7. Contour plots for velocity magnitude in the XY plane

Table 2. Variation in maximum Wall Shear Stress (WSS)

Fluid viscosity model	Newtonian	Case 1	Case 2	Case 3	Case 4	Case 5	Case 6
Maximum WSS [Pa]	279.84	279.84	234.58	234.58	235.00	238.71	242.74
Variation [%]	–	0	-16.17	-16.17	-16.02	-14.70	-13.26

4. CONCLUSIONS

The velocities of blood flow are directly impacted by the viscosity model, as observed in the simulations. Previous work indicates that the choice of rheology model may significantly affect the overall flow topology when the flow faces either large geometric variations (Almeida and Azevedo, 2018) or higher velocity gradients like in a flow at higher Reynolds numbers. In fact, the flow topology is affected by the choice of viscosity model even with a mild variation in geometry and for a flow at a low speed. In addition to the non-Newtonian behavior of the blood, the concentration of red blood cells in blood plasma and the region in which the blood is flowing may also lead the blood to behave nearly as a solid, indicating an increasing yield stress. Consequently, the application of a viscosity model sensitive to that is of fundamental importance. Although the differences in the velocity contours are fairly small in the simulations presented here, variations of up to 6.3% are obtained in the maximum velocity magnitude as the velocity profiles for the non-Newtonian fluids are flattened in relation to the Newtonian result. Depending on the region of interest and the flow regime, such variations in the maximum velocity magnitude may represent a result somewhat not acceptable or negligible.

The results for the unyielded Herschel-Bulkley fluid case presented good agreement with the power-law model regardless the small difference in the viscosity limits implementation in the source code. Additionally, the results of the GNF model also presented perfect match with the Newtonian fluid model. Such behavior is expected since the fluid index, $n = 1$, and consistency index, $k = \mu_{Newtonian}$, used in the GNF model for case 1 reconstitutes the Newtonian fluid model. The simulations demonstrated the sensitivity of the velocity magnitude as a function of the Bingham number. Moreover, the analysis presented here considered a steady state flow at very low Reynolds number, which would represent a single point in the cardiac cycle. The fact that the present simulations are considering steady state results implies no acceleration or deceleration of the flow and, therefore, the pulsatile nature of the blood flow is not represented by

the current results. Such analysis of the combined effects of non-Newtonian viscosity and pulsatile condition for more complex geometries is currently being performed and will be the subject of future work.

In summary, the authors, therefore, emphasize that the use of a non-Newtonian viscosity model and the choice of which non-Newtonian model to use are decisions that should be carefully addressed. Such a selection, combined with the correct choice of the appropriate model parameters, may be of fundamental importance in order to obtain more realistic and accurate results.

5. ACKNOWLEDGEMENTS

The authors gratefully acknowledge the partial support for the present research provided by Conselho Nacional de Desenvolvimento Científico e Tecnológico, CNPq, under the Research Grant No. 309985/2013-7. The authors are also indebted to the partial financial support received from Fundação de Amparo à Pesquisa do Estado de São Paulo, FAPESP, under the Research Grant No. 2013/07375-0. Acknowledgements are also necessary to Fundação Coordenação de Aperfeiçoamento de Pessoal de Nível Superior, CAPES, which provided a doctoral scholarship for the first author until May 2019. Finally, the authors further acknowledge CNPq and the Brazilian Petrochemical Company, BRASKEM, for the scholarship provided to the first author under the Grant No. 350176/2019-1.

6. REFERENCES

Almeida, G.P.V. and Azevedo, J.L.F., 2017. "Simulation of a 2-D pulsatile flow in a bifurcated geometry using open source software". In *24th ABCM International Congress of Mechanical Engineering*. Curitiba, PR.

Almeida, G.P.V. and Azevedo, J.L.F., 2018. "A study on the influence of rheology model in a constricted channel flow". In *17th Brazilian Congress of Thermal Sciences and Engineering*. Águas de Lindóia, SP.

Brambatti, V.M., 2010. *Utilização da Técnica de CFD Para Simulação do Escoamento de Sangue em Artéria Humana*. Master's thesis, Instituto Tecnológico de Aeronáutica, São José dos Campos, SP - Brazil.

Calafati, T.F., 2010. *Estudo do Escoamento em Artéria Parcialmente Obstruída Utilizando Técnicas de CFD*. Master's thesis, Instituto Tecnológico de Aeronáutica, São José dos Campos, SP - Brazil.

Cebral, J.R., Pergolizzi Jr., R. S. and Putman, C.M., 2007. "Computational fluid dynamics modeling of intracranial aneurysms: Qualitative comparison with cerebral angiography". *Academic Radiology*, Vol. 14, pp. 804–813.

Farina, A., Fusi, L., Mikelić, A., Saccomandi, G., Sequeira, A. and Toro, E.F., 2018. *Non-Newtonian Fluid Mechanics and Complex Flows*. Springer International Publishing.

Galdi, G.P., Rannacher, R., Robertson, A.M. and Turek, S., 2008. *Hemodynamical Flows*. Birkhäuser Basel.

Hirsch, C., 1990. *Numerical Computation of Internal and External Flows*. John Wiley.

Johnston, B.M., Johnston, P.R., Corney, S. and Kilpatrick, D., 2004. "Non-Newtonian blood flow in human right coronary arteries: Steady state simulations". *Journal of Biomechanics*, Vol. 37, No. 5, pp. 709–720.

Kim, S., 2002. *A Study of Non-Newtonian Viscosity and Yield Stress of Blood in a Scanning Capillary-Tube Rheometer*. Master's thesis, Drexel University, Philadelphia, PA.

Kim, S., Cho, Y.I., Jeon, A.H., Hogenauer, B. and Kensey, K.R., 2000. "A new method for blood viscosity measurement". *Journal of Non-Newtonian Fluid Mechanics*, Vol. 94, No. 1, pp. 47–56.

Mamun, K., Akhter, M.N., Mollah, M.S.H., Sheikh, M.A.N. and Ali, M., 2015. "Characteristics of pulsatile blood flow through 3-D geometry of arterial stenosis". *Procedia Engineering*, Vol. 105, No. Supplement C, pp. 877–884. The 6th BSME International Conference on Thermal Engineering.

Mittal, R., Seo, J.H., Vedula, V., Choi, Y.J., Liu, H., Huang, H.H., Jain, S., Younes, L., Abraham, T. and George, R.T., 2016. "Computational modeling of cardiac hemodynamics: Current status and future outlook". *Journal of Computational Physics*, Vol. 305, pp. 1065–1082.

Moukalled, F., Mangani, L. and Darwish, M., 2016. *The Finite Volume Method in Computational Fluid Dynamics - An Advanced Introduction with OpenFOAM and Matlab*. Springer International Publishing Switzerland, Switzerland.

OpenCFD, 2016. *OpenFOAM User Guide Manual*. OpenCFD Limited.

Paul, M. and Molla, M., 2012. "Investigation of physiological pulsatile flow in a model arterial stenosis using large-eddy and direct numerical simulations". *Applied Mathematical Modelling*, Vol. 36, No. 9, pp. 4393–4413.

Pinto, S.I.S., Doutel, E., Campos, J.B.L.M. and Miranda, J.M., 2013. "Blood analog fluid flow in vessels with stenosis: Development of an OpenFOAM code to simulate pulsatile flow and elasticity of the fluid". *APCBEE Procedia*, Vol. 7, pp. 73–79.

Piskin, S. and Celebi, M.S., 2013. "Analysis of the effects of different pulsatile inlet profiles on the hemodynamical properties of blood flow in patient specific carotid artery with stenosis". *Computers in Biology and Medicine*, Vol. 43, pp. 717–728.

Rosenfeld, M., 1993. "Validation of numerical simulation of incompressible pulsatile flow in a constricted channel". *Computers & Fluids*, Vol. 22, No. 2, pp. 139–156.

Tu, J., Inthavong, K. and Wong, K.K.L., 2015. *Computational Hemodynamics*. Springer Netherlands, Dordrecht, Nether-

lands.

Valencia, A., Botto, S., Sordo, J., Galvez, M. and Badilla, L., 2007. "Comparison of haemodynamics in cerebral aneurysms of different sizes located in the ophthalmic artery". *International Journal for Numerical Methods in Fluids*, Vol. 53, pp. 793–809.

Valencia, A., Zarate, A., Galvez, M. and Badilla, L., 2006. "Non-Newtonian blood flow dynamics in a right internal carotid artery with a saccular aneurysm". *International Journal for Numerical Methods in Fluids*, Vol. 50, No. 6, pp. 751–764.

Walburn, F.J. and Schneck, D.J., 1976. "A constitutive equation for whole human blood". *Biorheology*, Vol. 13, No. 3, pp. 201–210.

Weller, H.G., Tabor, G., Jasak, H. and Fureby, C., 1998. "A tensorial approach to computational continuum mechanics using object-oriented techniques". *Computers in Physics*, Vol. 12, pp. 620–631.

Wilcox, D.C., 2006. *Turbulence Modeling for CFD*. D C W Industries, La Canada, CA, 3rd edition.

Wong, G.K. and Poon, W., 2011. "Current status of computational fluid dynamics for cerebral aneurysms: The clinician's perspective". *Journal of Clinical Neuroscience*, Vol. 18, pp. 1285–1288.

7. RESPONSIBILITY NOTICE

The authors are solely responsible for the printed material included in this paper.